In vitro and *in silico* evaluation of the design of nano-phyto-drug candidate for oral use against *Staphylococcus aureus*

Yasemin Budama-Kilinc[1,2], Bahar Gok[3], Cigdem Cetin Aluc[3,4] and Serda Kecel-Gunduz[5]

[1] Bioengineering Department, Yildiz Technical University, Istanbul, Turkey
[2] Health Biotechnology Joint Research and Application Center of Excellence, Istanbul, Turkey
[3] Graduate School of Natural and Applied Science, Yildiz Technical University, Istanbul, Turkey
[4] Abdi Ibrahim Production Facilities, Abdi Ibrahim Pharmaceuticals, Istanbul, Turkey
[5] Physics Department, Istanbul University, Istanbul, Turkey

ABSTRACT

Onopordum acanthium is a medicinal plant with many important properties, such as antibacterial, anticancer, and anti-hypotensive properties. Although various studies reported the biological activities of *O. acanthium*, there is no study on its nano-phyto-drug formulation. The aim of this study is to develop a candidate nano-drug based on phytotherapeutic constituents and evaluate its efficiency *in vitro* and *in silico*. In this context, poly (lactic-co-glycolic acid) (PLGA) nanoparticles (NPs) of *O. acanthium* extract (OAE) were synthesized and characterized. It was determined that the average particle size of OAE-PLGA-NPs was 214.9 ± 6.77 nm, and the zeta potential was −8.03 ± 0.85 mV, and PdI value was 0.064 ± 0.013. The encapsulation efficiency of OAE-PLGA-NPs was calculated as 91%, and the loading capacity as 75.83%. The *in vitro* drug release study showed that OAE was released from the PLGA NPs with 99.39% over the 6 days. Furthermore, the mutagenic and cytotoxic activity of free OAE and OAE-PLGA-NPs were evaluated by the Ames test and MTT test, respectively. Although 0.75 and 0.37 mg/mL free OAE concentrations caused both frameshift mutation and base pair substitution ($p < 0.05$), the administered OAE–PLGA NP concentrations were not mutagenic. It was determined with the MTT analysis that the doses of 0.75 and 1.5 mg/mL of free OAE had a cytotoxic effect on the L929 fibroblast cell line ($p < 0.05$), and OAE-PLGA-NPs had no cytotoxic effect. Moreover, the interaction between the OAE and *S. aureus* was also investigated using the molecular docking analysis method. The molecular docking and molecular dynamics (MD) results were implemented to elucidate the *S. aureus* MurE inhibition potential of OAE. It was shown that quercetin in the OAE content interacted significantly with the substantial residues in the catalytic pocket of the *S. aureus* MurE enzyme, and quercetin performed four hydrogen bond interactions corresponding to a low binding energy of −6.77 kcal/mol with catalytic pocket binding residues, which are crucial for the inhibition mechanism of *S. aureus* MurE. Finally, the bacterial inhibition values of free OAE and OAE–PLGA NPs were determined against *S. aureus* using a microdilution method. The antibacterial results showed that the inhibition value of the OAE–PLGA NPs was 69%. In conclusion, from the *in vitro* and *in silico* results of the nano-sized OAE-PLGA NP formulation

Submitted 16 October 2022
Accepted 17 May 2023
Published 8 June 2023

Corresponding author
Yasemin Budama-Kilinc,
yaseminbudama@gmail.com

Academic editor
Sonia Oliveira

Additional Information and Declarations can be found on page 19

DOI **10.7717/peerj.15523**

produced in this study, it was evaluated that the formulation may be recommended as a safe and effective nano-phyto-drug candidate against *S. aureus*.

Subjects Bioinformatics, Biotechnology, Cell Biology, Microbiology, Molecular Biology
Keywords *O. acanthium* extract, PLGA nanoparticle, Antibacterial activity, Mutagenicity, Cytotoxicity, Molecular docking, MD

INTRODUCTION

Staphylococcus aureus is a dangerous organism that is a major cause of bacterial infections in community settings and hospitals (*Carter et al., 2020*). This pathogen is known to be more strongly associated with mortality than other bacterial pathogens. *S. aureus* can enter the bloodstream through cuts or open wounds in the skin, epithelium, or mucosal surface (*McCaig et al., 2006*). This leads to dangerous diseases, such as skin tissue infections, soft tissue infections, and debilitating and often fatal infections of the blood, bones, brain, and vital internal organs (*Crossley et al., 2009*; *Labreure, Sona & Turos, 2019*). For example, *S. aureus*, a deadly bacterium, causes bacterial abscesses in the body, such as endocarditis and lung infections, which can lead to a patient's death from heart failure (*Sibbald et al., 2006*).

Conventional antibiotics are available for treating *S. aureus* infections. However, multidrug-resistant strains of *S. aureus* are a major health hazard for humans and economic burden for governments because they are lethal (*Barman et al., 2016*; *Wang et al., 2017*; *Yang et al., 2017*). Additionally, there are many problems with the use of conventional antibacterial drugs, such as low water solubility and stability, low oral bioavailability, frequent drug administration, and toxicity (*Barman et al., 2016*; *Wang et al., 2017*; *Yang et al., 2017*). To address these issues, NPs have attracted much attention due to their physicochemical properties, drug targeting efficiency, increased uptake, and bio-distribution (*Eleraky et al., 2020*; *Karimi et al., 2016*). Among NPs, polymeric NPs are the most used because they have several advantages. They protect drugs from degradation, increase their solubility, and promote controlled release and drug targeting (*Kumari, Yadav & Yadav, 2010*).

PLGA is one of the most preferred polymers for preparing polymeric NPs, and it has been approved by the FDA as a biocompatible, biodegradable polymer. It is also widely used for research in the pharmaceutical industry as a desired drug carrier (*Abdollahi & Lotfipour, 2012*; *Kim et al., 2014*). Thanks to their controlled release properties (*Gaspar et al., 2018*; *Silva et al., 2014*), PLGA NPs contribute to more effective antimicrobial properties of the active substance with no degradation. They also have the potential for oral administration (*Hariharan et al., 2006*; *Mukerjee & Vishwanatha, 2009*). There are several reports in the literature on the oral use of PLGA NPs loaded with antimicrobial agents (*Abdollahi & Lotfipour, 2012*). Antimicrobial agents such as rifampicin, isoniazid, pyrazinamide, and ethambutol used orally against *Mycobacterium tuberculosis* were encapsulated with PLGA, and their antibacterial activity was evaluated (*Zhang et al., 2010*). The results showed that PLGA NPs loaded with antimicrobial agents improved

bioavailability and pharmacodynamics. In another study, the antibacterial activity of PLGA NPs loaded with azithromycin against *Salmonella typhi* was investigated. The results showed that azithromycin-loaded PLGA NPs were suitable for oral administration due to their favorable physicochemical properties and improved antimicrobial properties (*Mohammadi et al., 2010*).

The delivery of the antimicrobial agent to bacteria by NPs can occur *via* two mechanisms. In the first mechanism, the NP interacting with the cell wall or cell membrane carries the active substance into the target organism. The second mechanism is that the NPs adsorb to the cell wall and continue the release of antibacterial agents (*Agarwal, Kumar & Rajeshkumar, 2017*).

Plants have been used in traditional medicine in various cultures for many years. *O. acanthium* L. is an important herb used in medicine. This plant contains groups such as phenols, triterpenes, steroids (*Garsiya et al., 2019*), and biologically active compounds such as quercetin (*Koc et al., 2015*) and linoleic acid (*Arfaoui et al., 2014*). Due to its rich biologically active content of *O. acanthium* L., it is widely used in medicine.*O. acanthium* L. is used in traditional medicine as an anti-inflammatory, antitumor, and cardiotonic agent (*Garsiya et al., 2019*). Also, there is research in modern medicine on the properties of *O. acanthium*, such as bactericidal, cardiotonic, hypotensive, hemostatic, and antihypotonic (*Khalilov et al., 2003*; *Tyumkina et al., 2009*). In a study, the antibacterial properties of n-hexane and methanol extracts of *O. acanthium* seeds against Gram-positive bacteria (*S. aureus*, *S. epidermidis*, *M. loteus*) and Gram-negative bacteria (*E. coli* and *K. pneumonia*) were investigated by the MIC test (*Zare et al., 2014*). The methanol extract showed antibacterial activity against Gram-positive and Gram-negative bacteria. N-hexane showed no inhibitory activity against Gram-negative bacteria. In another study, the antibacterial activity of the leaf extract of *O. acanthium* was evaluated by MIC against *B. subtilis*, *X. euvesicatoria*, *L. plantarum*, and *A. fischeri* (*Móricz et al., 2017*). The results showed that the leaf extract had an antibacterial effect on the bacteria used.

In this study, OAE was encapsulated with PLGA and characterized. The average particle size, zeta potential, and polydispersity index values were determined using dynamic light scattering (DLS). The morphology of the OAE–PLGA NPs was demonstrated by SEM. The encapsulation efficiency, loading capacity, and *in vitro* release profile were determined using a UV-Vis spectrophotometer. The antibacterial effect of OAE–PLGA NPs against *S. aureus* was determined using the microdilution method. In addition, the antibacterial activity of the most abundant constituents of *O. acanthium* against *S. aureus* were investigated by molecular docking analysis to gain a better understanding of the mechanisms of action of these molecules. In addition, 50-ns MD simulation was performed to gain structural insight into the binding mode of the dynamic structure of the complex system. In the light of the information obtained from this study, it was revealed that quercetin in the OAE content interacted with the catalytic pocket binding residue, which is important for the inhibition of *S. aureus MurE*. Finally, the mutagenic and cytotoxic activity of free OAE and OAE-PLGA-NPs were evaluated by Ames test and MTT test.

MATERIALS AND METHODS

Materials

PLGA, dichloromethane (DCM) and polyvinyl alcohol (PVA), citric acid monohydrate, sodium dihydrogen phosphate monohydrate, 4-nitro-*o*-phenylenediamine (NPD), magnesium sulfate heptahydrate, potassium phosphate, D-biotin, sodium chloride, magnesium chloride hexahydrate, disodium hydrogen phosphate dihydrate, potassium chloride, Nutrient Broth (No 2), L-histidine, Dulbecco's Modified Eagle Medium (DMEM) and sodium ammonium phosphate tetrahydrate were purchased from Sigma–Aldrich (MO, USA). The *O. acanthium* extract (code: 5782ECH) was obtained from AZELIS TR KIMYA (Istanbul, Turkey). Agar was purchased from Difco (MD, USA). Muller-Hinton broth and Muller Hinton agar were purchased from Oxoid (Basingstoke, United Kingdom). Sodium azide was obtained from Merck (Darmstadt, Germany). HaCaT cell line was purchased from Thermo Fisher Scientific. 3-(4,5-Dimethylthiazol-2-yl)-2,5-Diphenyltetrazolium Bromide (MTT) was purchased from Biomatik. Fetal Bovine Serum (FBS) and Penicillin-Streptomycin (10X) Solution were purchased from Biological Industries.

Methods

Fabrication of OAE–PLGA NPs

PLGA NPs loaded with OAE were prepared using a double emulsification technique (*Budama-Kilinc, 2019b*; *Dewangan et al., 2022*; *Shabestarian et al., 2021*). A total of 100 mg of PLGA was dissolved in 6 mL of DCM. Then, 10 mg of OAE was dissolved in 2 mL of water and added to 2 mL of PLGA. The emulsion (w/o) was formed by sonication with 70 W energy for 3 min. Then, 10 mg of PVA was dissolved in distilled water. The obtained w/o emulsion was added dropwise to the PVA solution. Then, the formation of double emulsions (w/o/w) was started with the homogenization process, that is, the sonication of the mixture for 5 min at 70 kW. Subsequently, OAE–PLGA NPs were washed through three centrifugation cycles at 11,200*g* for 35 min, discarding the supernatant and re-suspending the pelletized NPs in deionized water. The NPs were filtered through a filter, which is a cellulose membrane with a pore size of 0.45 µm, and lyophilized in order to perform the DLS and SEM analyses and antibacterial activity and genotoxicity tests.

Preparation of the OAE standard curve

For this study, the standard curve of the OAE was determined using a UV-Vis spectrophotometer. Seven stock solution concentrations (1.5625; 3.125; 6.25; 12.5; 25; 50; 100 µg/mL) were prepared for OAE, and UV absorbance of all concentrations was measured at 323.8 nm triplicate for each sample. The absorbance graph was plotted against the curve concentration, and the equation was obtained as $y = 0.0033x$ ($R^2 = 0.9992$). The curve equation was used to determine both the encapsulation efficiency and the loading capacity (*Ercin et al., 2022*).

DLS analysis

The average particle size, polydispersity index (PdI), and zeta potential analyses of OAE–PLGA NPs were performed using a Zetasizer Nano ZS device (Malvern Instruments, Malvern, UK) equipped with a 4.0 mV He-Ne laser (633 nm) and operated at 25 °C.

FE-SEM analysis

The morphology of the OAE–PLGA NPs was demonstrated using FE-SEM (Apreo 2; Thermo Scientific, Waltham, MA, USA) (*Adedokun et al., 2022*). The sample containing OAE–PLGA NPs were dispersed in distilled water and placed in an ultrasonic bath for 45 min to sonicate. The sample was then prepared by dropping 10 µL of OAE–PLGA NPs onto the glass and drying at room temperature for 24 h. The sample was then placed in an ultrasonic bath. FE-SEM images were acquired using an in-lens detector at 100 kx magnification and 1.00 kV electron voltage.

Determination of encapsulation efficiency and loading capacity

The supernatant was taken after centrifugation of the OAE-loaded PLGA NPs to determine the encapsulation efficiency, and the amount of free OAE in the supernatant was calculated using an equation obtained from the OAE standard curve. The encapsulation efficiency was calculated using Eq. (1). The loading capacity for the OAE–PLGA NPs were calculated using Eq. (2).

$$EE\ \% = \frac{The\ total\ OAE - free\ OAE}{The\ total\ LEO} \times 100 \tag{1}$$

$$LC\ \% = \frac{The\ total\ OAE - free\ OAE}{Total\ Amount\ of\ the\ Nanoparticles\ Weight} \times 100 \tag{2}$$

In vitro release profile of OAE–PLGA NPs

The release of OAE from PLGA NPs was determined using the dialysis membrane method (*Budama-Kilinc, 2019b*; *Kumari, Tyagi & Sangal, 2022*). A total of 1 mg of OEA-PLGA NPs were suspended in 1 mL of distilled water and placed on pre-wetted dialysis membranes. The release was carried out in 100 mL of PBS (pH 7.4) medium in a shaking water bath maintained at 37 °C at 120 rpm. At fixed time intervals, the sample was taken from 1 mL of the release medium and added with an equal volume of buffer to keep the volume of the release medium constant. OAE amount in the release medium was analyzed using a UV-Vis spectrophotometer. The amount of OAE was calculated according to Eq. (3).

$$Release\ \ \% = \frac{Released\ Amount\ of\ \ OAE}{Total\ Amount\ of\ OAE} \times\ 100 \tag{3}$$

Antibacterial activity

The antibacterial activity of free OAE and OAE-PLGA NPs on *S. aureus* ATCC 25923 was evaluated by MIC assay. Bacterial culture was activated on Mueller–Hinton agar at 37 °C for 24 h. After then, three colonies were transferred to a fresh medium (MHB) to culture

the bacteria and grown overnight at 37 °C. The fresh bacterial culture was set to OD_{600} = 0.01 (5×10^6 cfu/mL). Free OAE and OAE-PLGA NPs were dissolved in distilled water, and serially diluted in MHB medium in 96-well plates to a final volume of 100 µL per well. Then, 5 µL of bacterial inoculum was added to each well. OAE-PLGA NP concentration was used in the range of 0.125 to 1 mg/mL, and free OAE concentration in the range of 0.093 to 0.75 mg/mL (the amount of OAE was calculated based on the amount loaded on the OAE-PLGA NPs). The experiment was performed in three technical replicates for each sample. The microplates were incubated at 37 °C for 24 h. The plates were analyzed at 540 nm with an ELISA reader (Multiskan GO Microplate Spectrophotometer; Thermo Scientific, Waltham, MA, USA) (*Khoshkhounejad et al., 2021*). Percentage inhibition of bacterial growth (%) was determined according to Eq. (4); A_c is the absorbance value of the negative control and A_t is the absorbance value of the samples.

$$Inhibition\ (\ \%) = \frac{A_c - A_t}{A_c} \times 100 \tag{4}$$

Molecular docking and MD analysis

The antibacterial efficacy of *O. acanthium*, which has anticancer, antioxidant, anti-inflammatory, analgesic, antipyretic, hypotensive, antiepileptic, wound-healing, and ACE inhibitory effects, was evaluated for the first time using molecular docking analysis. Antibacterial activity of OAE against *S. aureus*. was investigated at the molecular level.

The main structures formed by *O. acanthium* are flavonoids (such as apigenin, quercetin, and luteolin), phenylpropanoids, lignans, triterpenoids, sesquiterpene lactones, sterols, and three active antibacterial compounds, such as linoleic acid, linolenic acid, and germacranolide sesquiterpene lactone (*Al-Snafi, 2020*). Quercetin has been found in the aerial parts of the plant, the leaves, and the flowers. However, quercetin glycosides have also been isolated from herbs. In various extracts, such as ethanol, methanol, and acetone, the flowers contain 30 to 40 mg/L of quercetin. The leaves also contained 40 to 85 mg/L of quercetin. The main fatty acids in *O. acanthium* are linoleic acid (65.9%), oleic acid (18.8%), palmitic acid (5.8%), stearic acid (2.6%), and pentadecanoic acid (*Garsiya et al., 2019*; *Karl, Mueller & Pedersen, 1976*; *Koc et al., 2015*). The most abundant constituent of *O. acanthium* are quercetin and linoleic acid were preferred as the active ligands, and the protein data bank provided the crystal structure of *S. aureus* (PDB ID: 4C13) (*Ruane et al., 2013*) as the active receptor for performing molecular docking analysis. The Glide SP module of Maestro version 11.4 from Schrodinger Software (*Friesner et al., 2004*; *Halgren et al., 2004*) was implemented for molecular docking analysis and ADME calculations. The ChEBI service (*Hastings et al., 2016*) was used to generate the possible 3D molecular geometries of ligands. Both ligands that were considered possible inhibitors of *S. aureus* were transferred to the builder panel, and then the optimization process was performed using the LigPrep module. For energy minimization, the OPLS3 force field was used (*Harder et al., 2016*). For the docking analysis, the obtained geometries of the inhibitory ligands with the conformation with the lowest energy were used. The 3D crystal structure

of *S. aureus* MurE, which was obtained at a resolution of 1.9 and formed a single A-chain of 501 amino acids containing natural ligands, phosphate, potassium, chloride, and magnesium ions, was extracted from the protein database to perform the molecular docking analysis. Magnesium ions that were near the natural ligand were retained, while all water and ions that were not in the binding region of the natural ligand were deleted, as in the literature (*Azam, Saha & Jupudi, 2019*). Polar hydrogens were added, binding orders were assigned, and preprocessing was performed. Defective in the receptor structure were analyzed and loaded with PROPKA (*Olsson et al., 2011*) at pH 7.0. The receptor structure was optimized and minimized (*Sastry et al., 2013*) with the protein preparation tool using the OPLS3 force field. This process was performed, and it was expected that the root mean square deviation (RMSD) of the heavy atoms would converge to 0.30. By creating a 3D grid box centered on the center of gravity of each ligand, all residues containing thiol and hydroxyl groups were identified in the binding region of the receptor, and each ligand was docked to the receptor. Also, all pharmacokinetic and physicochemical properties of the different ligands binding to the same receptor were calculated using the Qik-Prop module (*Nija, Rasheed & Kottaimuthu, 2020*). The pharmacokinetic potential of both ligands thought to have inhibitory properties against *S. aureus*, such as molecular weight (M_W), percentage of oral absorption by humans, estimated octanol/water partition coefficient (QPlogPo/w), polar surface area (PSA), and Lipinski's Five Rules compatibility properties, were also obtained. Furthermore, to investigate effect of the most abundant constituent of *O. acanthium* on *S.aureus* by dynamic system and validate the stability of the complex, MD simulation (~13,820 water molecules and 49,119 atoms) was performed for 50 ns, and the DESMOND (*Bowers et al., 2006*; *Schrödinger, 2021*) module of the same program was used.

Ames/Salmonella assay

The Ames test was performed using the standard plate incorporation method (*Maron & Ames, 1983*; *Ying et al., 2022*; *Zhang et al., 2022*). TA98 and TA100 strains of *S. typhimurium* were used in the study.

After checking the genotypic characteristics of the test strains, including the histidine requirement, rfa mutation, plasmid pKM101, and uvr B mutation, the experiment was started (*Akin et al., 2016*). In the experiment, 0.25, 0.5, and 1 mg/plate concentrations of OAE-PLGA NPs were used, while free OAE concentrations were determined according to the loading capacity.

Briefly, 0.1 mL of the bacterial culture ($1–2 \times 10^9$) and the test sample were added to the top agar and mixed with a vortex. This mixture was then poured onto the surface of a minimal glucose agar (MGA) plate. The plates were incubated at 37 °C for 48 h. After incubating the plates, mutagenicity was assessed by comparing the number of revertant colonies formed by the tested samples with the number of revertant colonies formed on the negative plates. Experiments were performed in triplicate for each sample.

MTT assay

Cytotoxicity of free OAE and OAE–PLGA NPs were determined by MTT test. Briefly, L929 cells were seeded in 96-well plates (1×10^4 cells/well) and OAE and OAE–PLGA NPs were applied after 24 h of culture. OAE–PLGA NPs concentrations were determined as 0.125, 0.25, 0.5, 0.75, 1 and 2, mg/mL, while concentrations for free OAE was applied according to the loading efficiency. After treatment, cells were cultured for 24 h in a 37 °C humidified 5% CO_2 incubator. After 24 h, 5 mg/mL MTT was added to each well, and cells were incubated for 4 h in a 37 °C 5% CO_2 incubator. Then the supernatant was removed and 100 µL of DMSO was added. The plate was measured using an ELISA reader (EPOCH; Biotek, Winooski, VT, USA) at 570 nm. Mean optical density (OD) values were used to estimate cell viability. Cell viability was calculated using Eq. (5).

$$\text{Cell viability} \quad \% = \frac{\text{OD of Experimental Group}}{\text{OD of Control Group}} \times 100 \tag{5}$$

Statistical analysis

Statistical analysis of the mutagenicity and cytotoxicity study was performed using one-way analysis of variance (ANOVA) to compare values between control and treated groups. Values showing $p < 0.05$ were considered statistically significant.

RESULTS AND DISCUSSION

Characterization results of OAE-PLGA-NPs

DLS analysis

The hydrodynamic size, distribution, and surface charge of NPs were determined using DLS, the most widely used method for NP characterization (*Budama-Kilinc, 2019a*; *Egil et al., 2020*; *Nemati et al., 2022*; *Samling et al., 2022*). In this study, the average size, polydispersity index (PdI), and zeta potential of OAE–PLGA NPs were measured using DLS principles.

The DLS result of OAE–PLGA NPs was shown in Fig. 1. It was found that the average particle size was 214.9 ± 6.77 nm and the zeta potential was −8.03 ± 0.85 mV.
The OAE–PLGA NPs exhibited a narrow size distribution with PdI values of 0.064 ± 0.013.

NPs are particles with a size of less than 100 nm (*Borm et al., 2006*; *Dowling, 2004*). However, the size of polymeric NPs ranges from 10 to 1,000 nm, and they are used in various applications (*Gheffar et al., 2021*; *Hamzaoui & Laraba-Djebari, 2021*; *Ni et al., 2021*; *Roberts et al., 2020*). The double emulsion method allows the preparation of NPs with a size larger than 100 nm in the synthesis of polymeric NPs (*Dorjsuren et al., 2020*; *Pieper & Langer, 2017*; *Sousa et al., 2017*). The size of OAE–PLGA NPs synthesized by the double emulsion method was compatible with the particle sizes synthesized in previous studies.

The PdI value is a measure of the homogeneity of NP size. A PdI value close to zero indicates a homogeneous distribution, while a PdI value close to one indicates a completely heterogeneous and polydisperse particle population (*Al-Mahallawi, Abdelbary & Aburahma, 2015*; *Gebreel et al., 2021*). In our study, it was found that the PdI values of the

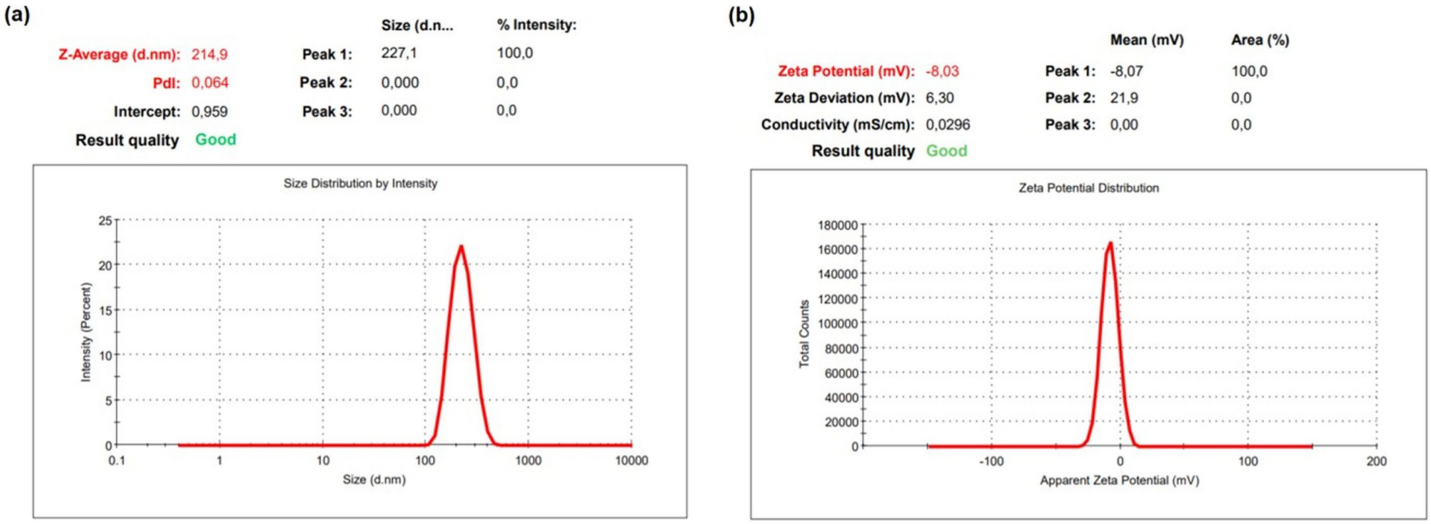

Figure 1 DLS analysis. DLS analysis of OAE–PLGA NPs: (A) average particle size graph, (B) zeta potential graph.
Full-size DOI: 10.7717/peerj.15523/fig-1

synthesized OAE–PLGA NPs were smaller than 0.1. This result indicates that the OAE–PLGA NPs have good homogeneity and uniform particle size distribution.

The zeta potential is the total charge acquired by particles in a given medium. This charge value is an indication of the potential physical stability of NP distribution (*Dhas, Ige & Kudarha, 2015*). The electric charge of the OAE–PLGA NPs were negative due to the terminal carboxyl groups in PLGA (*Bacanli et al., 2021*; *Budama-Kilinc, 2019b*; *Zhang et al., 2021*).

Encapsulation efficiency and loading capacity

Encapsulation is a strategic method to keep drug molecules stable and increase their efficacy. Therefore, encapsulation efficiency and loading capacity are essential calculations and measurements for NP preparation (*Shen et al., 2017*). Standard curve equation of OAE was $y = 0.0033x$ ($R^2 = 0.9995$). The encapsulation efficiency was calculated to be 91% using Eq. (1), and the loading capacity was determined to be 75.83% using Eq. (2). The results of encapsulation efficiency and loading capacity show that OAE was encapsulated and that OAE–PLGA NPs were successfully obtained.

In vitro release kinetics of OAE–PLGA NPs

In vitro release kinetics are crucial as an indicator of the pharmacokinetic and pharmacological effects of a drug *in vivo* (*Abdelkader et al., 2020*). The *in vitro* release kinetics of OAE–PLGA NPs were performed in PBS buffer (pH = 7.4) using the dialysis membrane method (*Folle et al., 2021*) and monitored for 144 h. The percentage of OAE released as a function of time was given in Fig. 2. The results showed that 58.18% of OAE was released within 9 h, 64.24% within 24 h, and 99.39% within 144 h. The *in vitro* release profile of the OAE–PLGA NPs showed a biphasic release pattern. The initial rapid release may be attributed to the rapid release of OAE entrapped near the surface of the NPs.

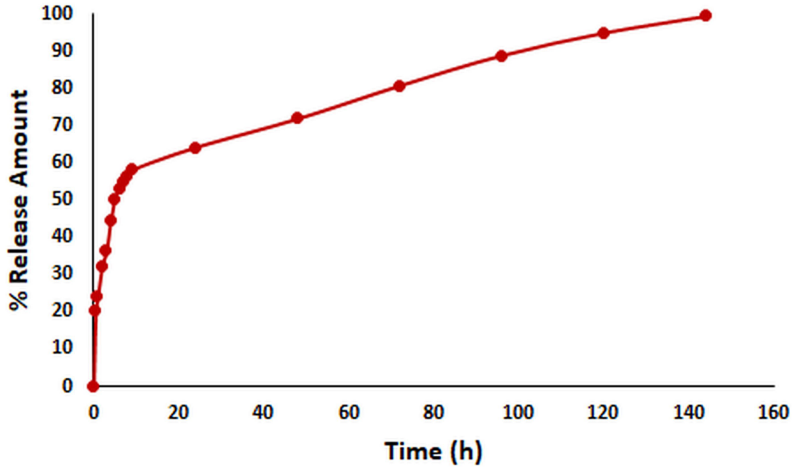

Figure 2 ***In vitro*** **release study result.** *In vitro* release profile of OAE-PLGA NPs.
Full-size DOI: 10.7717/peerj.15523/fig-2

However, the sustained release could be related to the OAE entrapped deep in the core of the PLGA NPs (*Chourasiya, Bohrey & Pandey, 2016*; *Radwan et al., 2021*).

FE-SEM analysis

The morphology of the OAE–PLGA NPs and blank PLGA NPs were observed using FE-SEM (Fig. 3). As shown in the figure, both NPs (Figs. 3A and 3B) were spherical morphology with a homogeneous distribution were produced (*Adedokun et al., 2022*; *Malewicz et al., 2022*).

Antibacterial activity assay

The antibacterial activity of free OAE and OAE–PLGA NPs were examined using the broth microdilution method. The bacterial growth inhibition of free OAE and OAE–PLGA NPs on *S. aureus* was 99% and 69%, respectively (Table 1).

Radwan et al. (2021) reported that the encapsulation of the drug with PLGA NPs resulted in a significantly slower and more controlled drug release compared with the free drug. This explains the lower antibacterial activity compared to free OAE, considering the amount of OAE released from the NPs in the first 24 h (64%). Our results are compatible with the literature (*Chaudhary & Kumar, 2014*; *Hill, Taylor & Gomes, 2013*; *Mohammadi et al., 2010*; *Simon et al., 2020*).

OAE contains active compounds such as quercetin (*Koc et al., 2015*) and linoleic acid (*Matthaus, Ozcan & Al-Juhaimi, 2014*). Many studies in the literature have reported the antibacterial activity of quercetin (*Kost et al., 2020*; *Shu et al., 2011*) and linoleic acid (*Bentrad, Gaceb-Terrak & Rahmania, 2017*; *Jummes et al., 2020*; *Kusumah et al., 2020*). The antibacterial activity shown by OAE could be due to these active compounds.
The antibacterial mechanism of quercetin can be used in several ways. These mechanisms include alteration of cell permeability, harm to the bacterial cell wall, and inhibition of nucleic acid synthesis, which may lead to altered protein synthesis and decreased enzyme activities (*Wang et al., 2018*). The target of the antibacterial mechanism of linoleic acid is

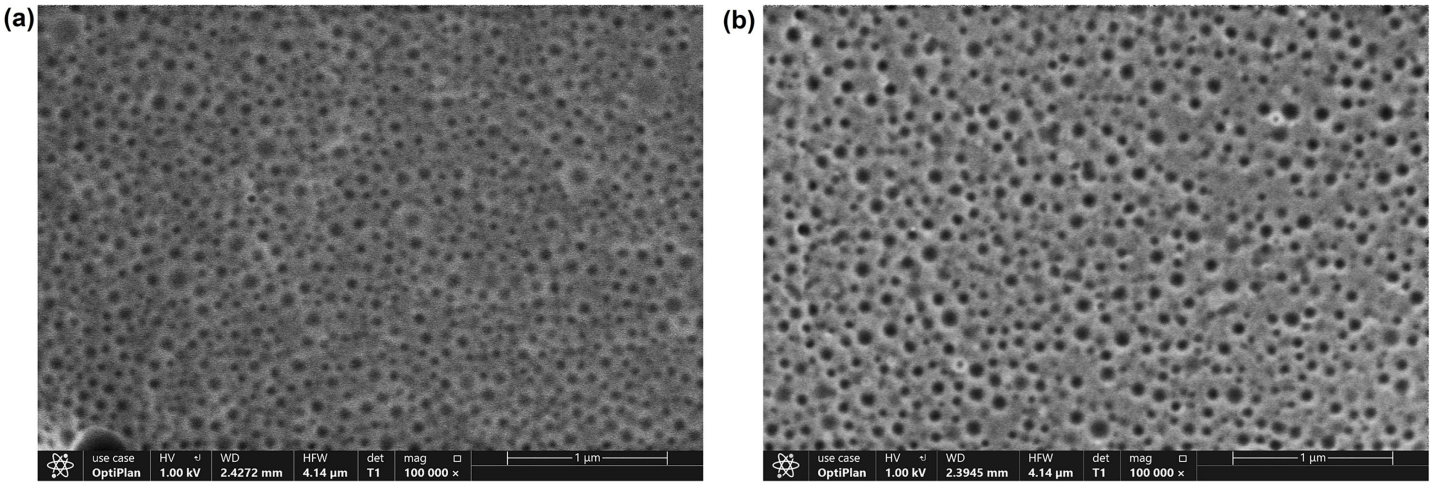

Figure 3 FE-SEM analysis. FE-SEM image of blank PLGA NPs (A), OAE-PLGA NPs (B). Full-size DOI: 10.7717/peerj.15523/fig-3

Table 1 Antibacterial activity assay results. The MIC and inhibition values of OAE and OAE–PLGA NPs.

Treatment	Concentration	% Inhibition ± SD	MIC (mg/mL)
Free OAE	0.75	99.0 ± 0.032	0.75
	0.37	93.4 ± 0.016	
	0.18	68.5 ± 0.034	
	0.093	45.6 ± 0.065	
OAE-PLGA-NPs	1	69.0 ± 0.001	>1
	0.5	67.7 ± 0.007	
	0.25	65.4 ± 0.013	
	0.125	59.4 ± 0.007	

the cell membrane. Linoleic acid dissolves the cell membrane and allows cell metabolites to leak out and the cells to break down (*Desbois & Smith, 2010*).

Molecular docking and MD analysis results

Molecular docking analysis was performed to model the possible binding conformations of active compounds, such as quercetin and linoleic acid in *O. acanthium* against *S. aureus*. Based on the molecular docking analysis, the binding affinity to the target receptor and the potential of the binding compounds to become drugs can be predicted. While binding affinity is expressed by the value of the docking score, lower values for binding affinity mean that a compound requires less energy to bind, *i.e.*, its potential to bind to the target receptor is higher (*Baker et al., 2007*; *Tassa et al., 2010*). The binding affinities were determined and compared for quercetin and linoleic acid in *O. acanthium* against *S. aureus*. in Table S1. The binding conformation of the two ligands, such as quercetin (Fig. 4A) and linoleic acid (Fig. 4C), with the highest binding affinity, and the hydrogen bonding interactions between quercetin (Fig. 4B) and linoleic acid (Fig. 4D) against the *S. aureus*

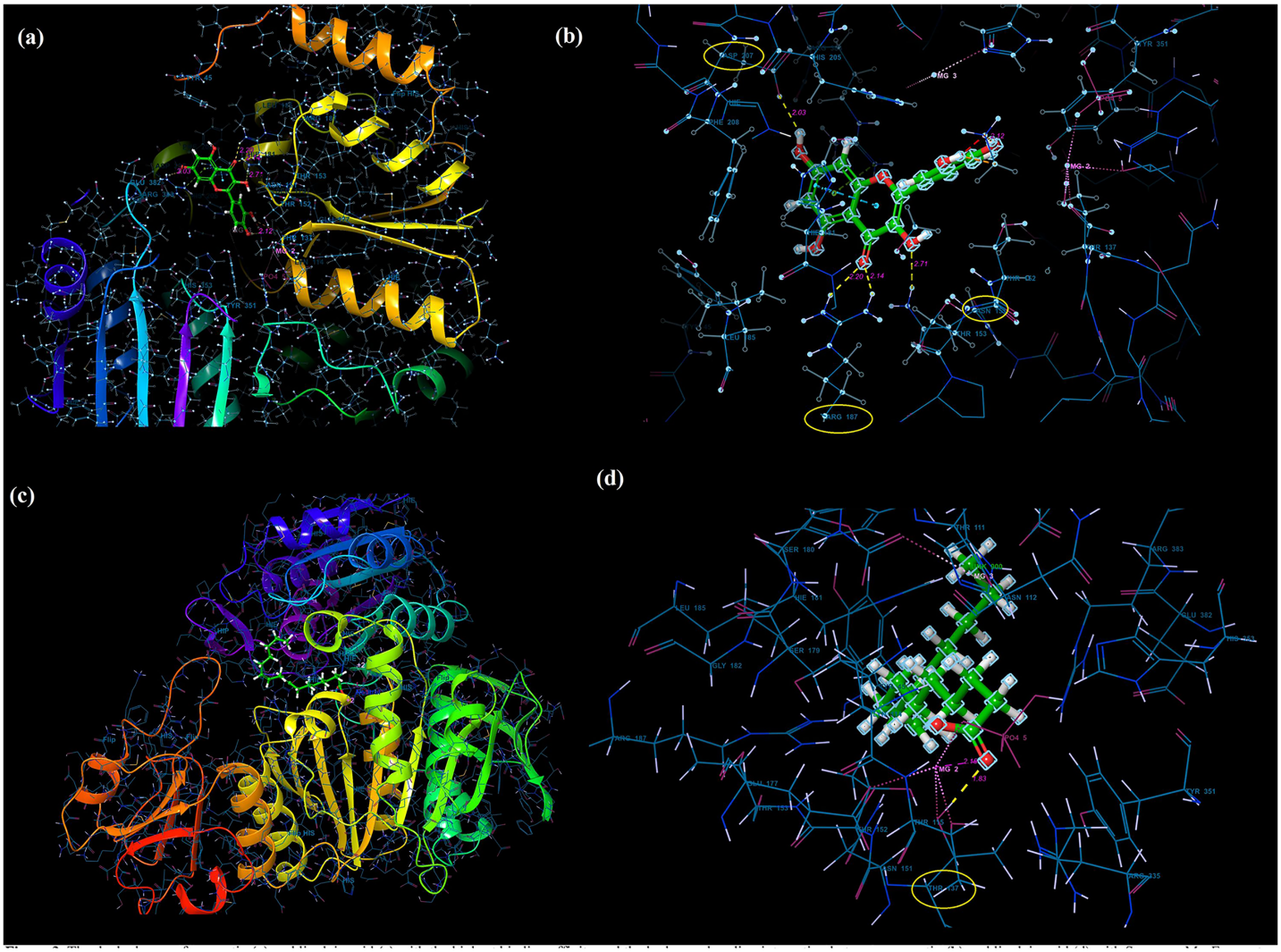

Figure 4 Molecular docking results. Docked pose of quercetin (A) and linoleic acid (C) with the highest binding affinity and hydrogen bonding interactions between quercetin (B) and linoleic acid (D) with the *S. aureus* MurE receptor. Full-size DOI: 10.7717/peerj.15523/fig-4

MurE receptor were shown in Fig. 4. The more negative the docking score, the stronger the binding affinity of the ligand to the receptor. In inhibiting *S. aureus*, quercetin had the lowest docking score of −6.770 kcal/mol. Quercetin is known as penta hydroxy flavone a form the flavonoid group and has five hydroxyl groups in its structure. Because of the five hydroxyl groups, it was very well bound to the active binding site of *S. aureus* MurE. Linoleic acid is known as cis, cis-9,12-octadecadienoic acid and has only one binding carboxyl group. *S. aureus* is an important human pathogen and is among the leading causes of skin and soft tissue and device-related infections, as well as infective endocarditis. The *S. aureus* MurE enzyme is one of the potential targets for the development of new therapeutic agents due to its high substrate specificity and ubiquitous nature among bacteria (*Azam, Saha & Jupudi, 2019*). The residues and binding types where both ligands bind to the active binding site of the *S. aureus* receptor are also shown in Fig. 5.

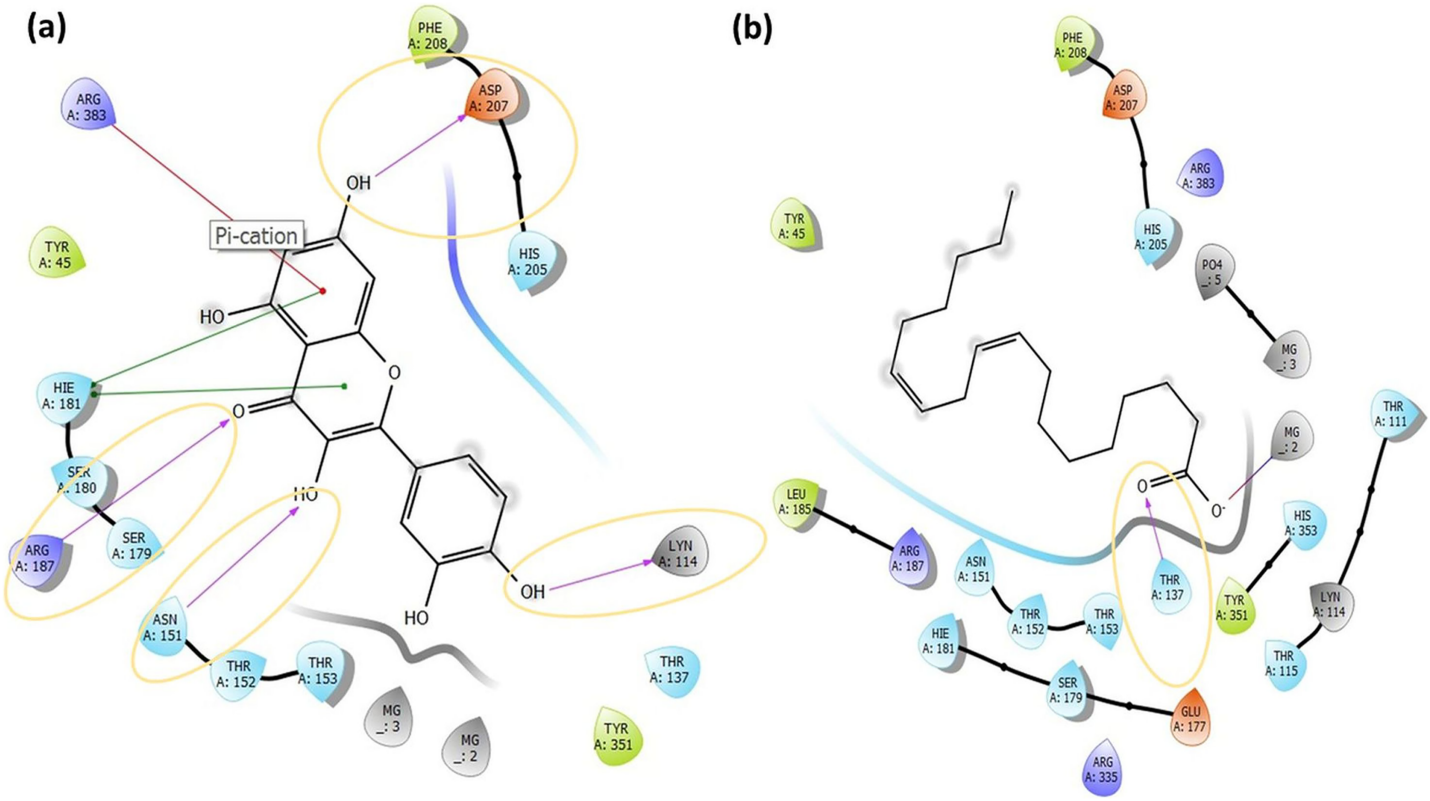

Figure 5 The active binding sites and the 2D ligand interactions. The 2D binding interactions with quercetin (A) and linoleic acid (B) major compounds in *O. acanthium* with the active binding site of *S. aureus* MurE. Full-size DOI: 10.7717/peerj.15523/fig-5

The higher affinity value of quercetin is due to the fact that the OH and O atoms of quercetin, as shown in Fig. 5A, interact harmoniously with the corresponding residues at the active binding site of the receptor. Three hydroxyl groups and one oxygen atom in quercetin were connected to the residues (ASP207, ASN151, LYS114, and ARG187) at the active binding site *via* hydrogen bonds (2.03, 2.71, 2.12, 2.14 and 2.20 Å), as shown in Table S1. In a study on the *Staphylococcus aureus* MurE inhibitor, it was observed that the molecule whose inhibitory activity was investigated provides this activity by making hydrogen bonds with the active binding site of the similar residues with ASN151, THR152, SER180, ARG187 AND LYS219 (*Azam, Saha & Jupudi, 2019*). These hydrogen bonding interactions are considered important interactions for the stabilization of the inhibitor within the catalytic pocket of *S. aureus* MurE.

Quercetin made also strong hydrogen bonds with the similar residues ASN151 and ARG187, which are available in domain 2 region covering from 99 to 332 residues to the active binding site of *Staphylococcus aureus* MurE in Fig. 5A. The powerful interactions that supported stronger binding were also two pi-pi stacking interactions between the benzene rings of quercetin and the HIE181 residue and a pi-cation interaction between the benzene ring with the ARG383 residue. Non-covalent interactions between the aromatic rings of quercetin and HIE181, as well as an electron-rich pi system and an adjacent cation, such as ARG383, contributed to the stronger binding seen in Fig. 5A. Apart from the

noncovalent interaction from ARG383 residue at domain 3 which consists of residues from 333 to 493, hydrogen bonding interactions in the binding pocket of domain two appeared to play a important role for the stabilization of the inhibitor.

Linoleic acid was also bound to the active binding site with an energy of −2.734 kcal/mol. Figure 5B built a hydrogen bond interaction (1.83 Å) between the oxygen atom and the THR137 residue and a salt bridge (2.16 Å) interaction between the oxygen atom of the carboxyl group and the magnesium ion.

Figures S1A and S1B shows the molecular electrostatic potential surface of the binding pocket of the *S. aureus* MurE receptor and ligands for quercetin (Fig. S1C) and linoleic acid (Fig. S1D), respectively. Considering the difference between the binding affinity energy values and the extent of interaction at the active binding site, quercetin was found to have more effective binding than linoleic acid, so that quercetin has a stronger inhibitory effect on *S. aureus* than linoleic acid. *In silico* molecular docking analysis results show that *O. acanthium* extract is promising as a drug candidate with strong antibacterial activity against *S. aureus*, due to the quercetin compound, whose antibacterial activity has also been proven in the literature and presented in this study. The ADME properties, which determine the kinetics of drug exposure in tissues and establish the performance and pharmacological activities of the active ingredients as drugs, were calculated for quercetin and linoleic acid in *O. acanthium*, and the results were shown in Table S2. Quercetin and linoleic acid both have a low molecular weight. While quercetin has four donors and five acceptors, linoleic acid contains only one donor and two acceptors. The calculated Caco-2 and MDCK permeability values for linoleic acid were in the medium range, but for quercetin, they were poor.

In order to gain insight into the inhibitor mechanism by dynamic interaction of OAE's active compound, such as quercetin, on *S. aureus* MurE receptor and its stability, RMSD and RMSF were analyzed relative to the initial structure by subjecting to the 50-ns simulations. Figure 6A presents the *S. aureus* MurE receptor backbone RMSDs for Cα with green and ligand RMSD with pink.

According to the MD analysis, during the first 5 ns step, calculated RMSD values of the protein backbone Cα indicated updraft from 1.2 and to 1.8 Å and remained stable around 2.1 Å for the remaining simulation time. At the same time, it was seen that the calculated ligand RMSD value increased from 0.3 to 0.8 Å under 10 ns and remained stable around 0.8 Å for the next 40 ns. This balance RMSD value indicated that the entire complex is in equilibrium. In Fig. 6B, the peaks are expressed by the protein domains that fluctuate the most during simulation, while the residues interacting with the inhibitory structure are also represented by green vertical lines. For the backbone, these fluctuation values seem to increase from 1.5 to 3.0 Å for the first 100 residue indexes. The backbone and Cα value of the catalytic pocket residues (99–332 residues) bound to the inhibitor exhibited root mean square fluctuation (RMSF) values are in the range of 0.55–1.45 Å, respectively.

Trajectory analysis from the MD simulation revealed hydrogen bonding, hydrophobic, and ionic interactions of the inhibitor with the key binding residues of the catalytic pocket, as seen in Fig. 6C. Consistent with the results of the docking analysis, hydrogen bonds were observed with ASN151, THR152, LYS114, ARG383 and LYS219 which formylated at

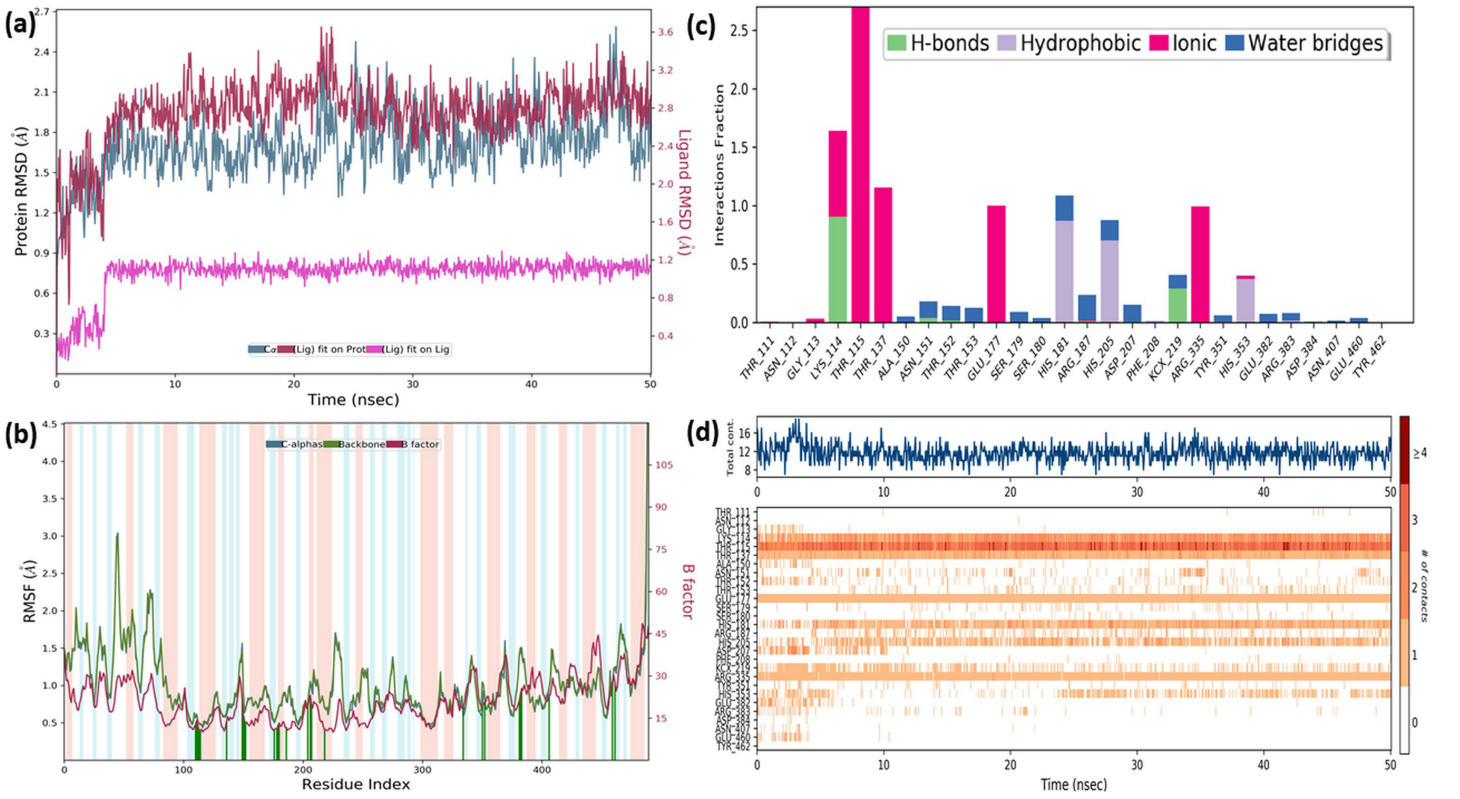

Figure 6 **MD results.** RMSD profile of Cα (A), RMSF profile of 4C13 residues (B), interactions fraction diagram of quercetin (C), interaction counts profile of quercetin with different residues of 4C13 (D), during 50 ns MD. Full-size DOI: 10.7717/peerj.15523/fig-6

KCX219 in Figs. 6C and 6D, while ionic interactions were observed with GLY113, LYS114, THR115, THR137, GLU177 and ARG335. In complex structure, water-bridged interactions were observed between amino acid regions between ALA150, ASN151, THR152, SER179, ARG187, ASP207, TYR351, GLU382, ARG383 and GLU460, while hydrophobic interactions occurred in HIS181, HIS205 and HIS353 regions.
The interaction counts and times of the inhibitor with the relevant residues are also seen in Fig. 6D. Interactions with THR115, LYS114, THR137, GLU177, ARG335 are expressed as interactions that exist during the 50 ns MD period.

The RMSF values of the atoms of the inhibitor are also given in Fig. 7A. Accordingly, the atoms that act together with the protein in the Ligand are given with their numbers. The hydroxyl group, defined by atomic number 22, was in water-mediated ionic interactions with ARG335, THR115, and THR137 (99%, 72%, and 100% of the MD trajectory, respectively). The hydroxyl oxygen of the same moiety formed a strong hydrogen bond of 88% of the MD trajectory with LYS114. Again, the same hydroxyl group made ionic interaction with GLU177 *via* the magnesium cation at 100% of the MD trajectory. In addition, pi-pi interactions with HIS181, HIS205 and HIS353 occurred of 65%, 69% and 37% of MD trajectory, respectively seen in Fig. 7B.

It is evident from above results that the strong hydrogen bonding interactions with LYS114 and LYS219 in Figs. 6C and 7B, and other hydrogen binding with ASN151 and

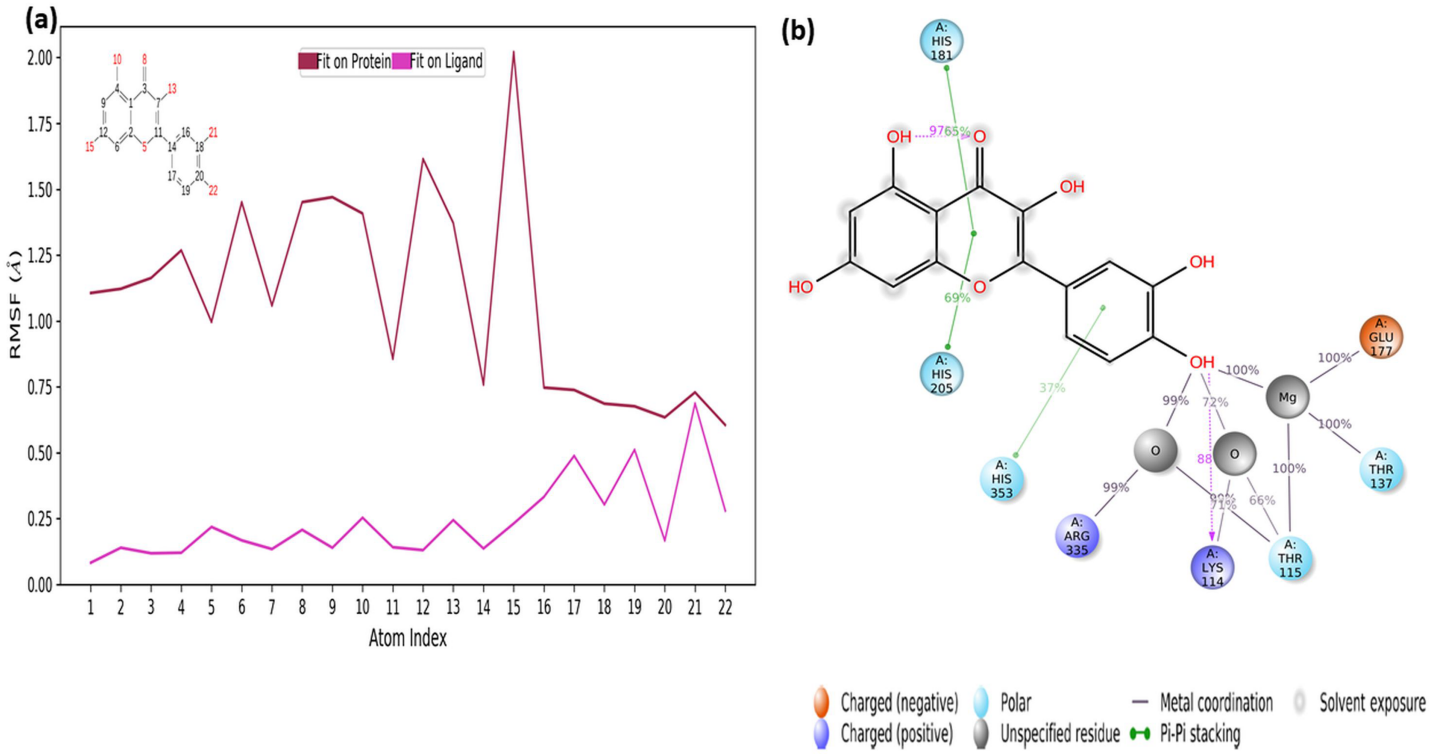

Figure 7 RMSF profile of quercetin. RMSF profile of atom of quercetin (A) interactions diagram of quercetin (B) with different residues of 4C13, during 50 ns MD.
Full-size DOI: 10.7717/peerj.15523/fig-7

THR152 in Fig. 6C, and also ionic interactions with THR115, THR137, GLU177 and ARG 335 and pi-pi interactions with HIS181, HIS205 and HIS353 are crucial for enhancing the activity value.

Ames/Salmonella assay

The Ames test is a real-time, sensitive, short-time test that represents the mutagenicity of chemical substances (*Abdul Majid et al., 2022*; *Coppi et al., 2022*; *Tsai et al., 2020*; *Zhao et al., 2020*). This test system is frequently used to investigate the mutagenicity of many chemical substances. There are different tests to measure whether mutation or genetic damage is present in microbial and mammalian cells, but the Ames test still plays an important role in testing chemicals for commercial use (*Zeiger, 2019*). Many strains of *S. typhimurium* (TA100, TA98, TA97, TA102, TA1535, TA 1537, and TA1538) were used for the Ames test. There are different mutations in the genes of these strains.
S. typhimurium strains TA98 and TA100 are the most standardized strains against frameshift and base pair change mutations (*Mortelmans & Zeiger, 2000*). Therefore, the *S. typhimurium* TA98 and TA100 strains were used in this study. The mutagenicity results of free OAE and OAE–PLGA NPs were shown in Fig. 8. The results showed that the applied concentrations of OAE–PLGA NPs were not mutagenic ($p > 0.05$). However, 0.75 and 0.37 mg/mL concentrations of free OAE were found to cause both frameshift mutation (TA98) and base-pair substitution (TA100) ($p < 0.05$).

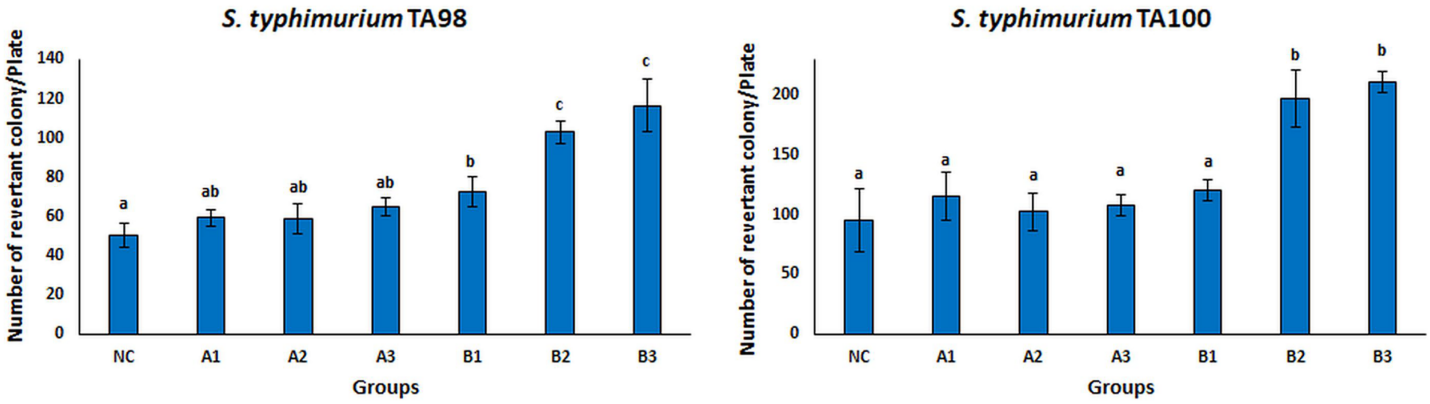

Figure 8 Mutagenicity results. Mutagenicity results of free OAE and OAE-PLGA NPs. NC, Negative control; A1, 0.25 mg/Plate of OAE-PLGA NPs; A2, 0.5 mg/Plate of OAE-PLGA NPs; A3, 1 mg/Plate of OAE-PLGA NPs; B1, 0.17 mg/plate of free OAE; B2, 0.38 mg/plate of free OAE; B3, 0.75 mg/plate of free OAE.
Full-size DOI: 10.7717/peerj.15523/fig-8

The fact that free OAE causes a mutagenic effect ($p < 0.05$) and that OAE–PLGA NPs have no mutagenic effect could be explained by the controlled release system.
The controlled release system provides a much slower drug release. This eliminates the mutagenic effect. Many studies in the literature report that the toxicity of the drug is eliminated thanks to the controlled release system (*Sousa et al., 2017*; *Zhang et al., 2021*). The absence of any mutagenic effect of OAE–PLGA NPs tested on mutant strains of TA 98 and TA 100, two bacterial species, confirms the safety of these particles for use in diseases caused by *S. aureus* bacteria (*Ballesteros-Ramírez, Durán & Fiorentino, 2021*; *Khan et al., 2021*).

MTT assay

One of the most used tools in toxicity studies associated with nanoparticle-based therapies is cell cultures. They are simple, cost-effective, and do not pose any ethical problems. In addition, *in vitro* cell tests allow checking of the cellular environment and homogeneity, both morphologically and compositionally. This provides a deeper understanding of the biological and biochemical processes that occur during treatments (*Razura-Carmona et al., 2022*). L929 mouse fibroblast was used for *in vitro* cytotoxicity testing in this study. This cell line is often preferred by researchers because it is easy to control cell culture conditions (*ISO, 2009*) and responds more sensitively than primary cells (*Nabavizadeh et al., 2022*; *Sharma et al., 2022*). The results of cytotoxicity analysis on L929 fibroblast treated with free OAE and OAE-PLGA-NPs were given in Fig. 9. OAE-PLGA-NPs did not show cytotoxicity against fibroblast cells even at the highest concentration of 2 mg/mL ($p > 0.05$). However, 0.75 and 1.5 mg/mL concentrations of free OAE were cytotoxic to fibroblast cells ($p < 0.05$).

Paszel-Jaworska, Romaniuk & Rybczynska (2014) *Ziziphora clinopdioides* Lam. theoretically attributed the toxic effect of ethanolic extract (EEZC) to the chemical content of the extract. OAE's toxicity may be due to its chemical content. *Omokhua et al. (2018)* reported that the antibacterial and antifungal activity of *Tithonia diversifolia* belonging to the Asteraceae family may be due to the toxicity of the plant extract. This may explain the

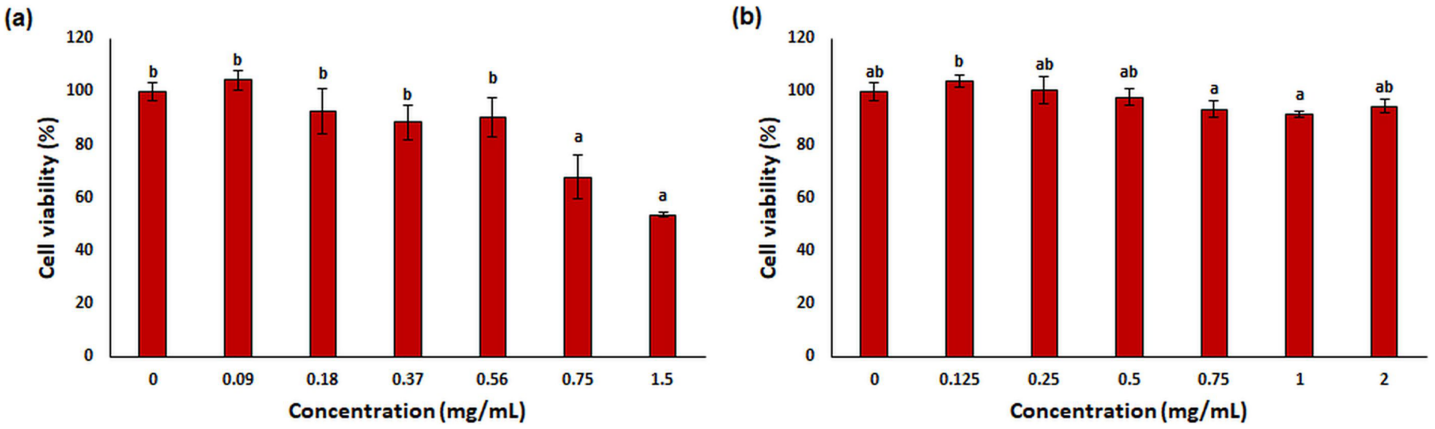

Figure 9 The cytotoxicity results. The cytotoxicity results (A) free OAE and (B) OAE-PLGA NPs. Different letters mean significant differences between the sample and control. Full-size DOI: 10.7717/peerj.15523/fig-9

antibacterial effect of *O. acanthium* extract (OAE) belonging to the Asteraceae family on *S. aureus*.

In our study, the toxicity of free OAE and OAE-PLGA-NPs were evaluated with two different tests. While OAE-PLGA-NPs did not cause toxicity in both test systems ($p > 0.05$), high concentrations of free OAE caused toxicity ($p < 0.05$). However, the concentration of 0.37 mg/mL was toxic ($p < 0.05$) in the Ames/Salmonella test, while it was non-toxic in the MTT test ($p > 0.05$).

Taherkhani (2015) reported that essential oil components have a very different mode of action in bacteria and eukaryotic cells. While they have potent bactericidal properties for bacterial cells, they alter apoptosis and differentiation in eukaryotes, interfere with post-translational modification of cellular proteins, and induce or inhibit some hepatic detoxifying enzymes. Therefore, they emphasized that essential oils could cause very different effects in prokaryotes and eukaryotes. OAE contains various components (*Al-Snafi, 2020*). These components may have caused different effects on prokaryotic and eukaryotic cells, such as essential oils.

CONCLUSION

S. aureus, a human commensal microbe, has caused infections throughout history and is likely to continue to be a significant cause of human infections. The ability of *S. aureus* to rapidly develop antibiotic resistance provides an orientation towards alternative treatment methods for severe *S. aureus* disease. The resistance of *S. aureus* to existing antibiotics is both a serious health threat and an economic burden. Therefore, new antibacterial agents and innovative systems, such as nano-sized formulations with controlled release features, are urgently needed.

In literature studies, it has been found that delivery systems based on nanomaterials as drug carriers show great potentials in antibacterial therapy. Functional nanomaterials with antibacterial properties do not induce bacterial resistance and can suppress bacterial resistance by bypassing drug-resistant mechanisms while protecting important structural components of loaded antibiotics. Nanoparticle formulations are often preferred because

of their properties that protect the antibacterial agent and increase its biocompatibility. In addition, nanoformulations can increase drug-induced antibacterial activity by promoting interaction with bacteria and/or increasing the targeting capacity of drugs. They may lead to an effective result with the use of less active drug substance.

Plants as antibacterial agents are used in the traditional medicine of different cultures. *O. acanthium* L. is an important plant widely used for its bactericidal properties. Although there are several studies in the literature proving the antibacterial properties of *O. acanthium* L., there is no study in which *O. acanthium* L. was encapsulated for oral use.

In this study, OAE–PLGA NPs were developed for use as a controlled drug system for oral administration against *S. aureus*. The antibacterial activity of OAE encapsulated with PLGA polymer was low compared to that of free OAE. However, the Ames and MTT tests revealed that free OAE was toxic. The mutagenicity and cytotoxicity of free OAE were eliminated after coating with PLGA. The results indicate that the PLGA NPs system improves the biocompatibility of free OAE and could be a useful approach for oral delivery against *S. aureus*. Our docking analysis results show that Quercetin in the OAE extract performed strong hydrogen bonding interactions with ASN151 and ARG187 residues in the catalytic pocket of *S. aureus MurE*, and these interactions are important interactions for enzyme inhibition. The MD simulation analysis also provides a study of the binding mode of the quercetin-based inhibitor against the *S. aureus MurE* enzyme. Quercetin formed hydrogen bond interactions with catalytic pocket binding residues LYS114, ASN151, THR152 and LYS219, which are crucial for the inhibition mechanism of *S. aureus MurE*.

ACKNOWLEDGEMENTS

The authors are thankful to have had access to the laboratory infrastructure of the Applied Nanotechnology and Antibody Production Laboratory established by TUBITAK (Projects 115S132 and 117S097). The authors are also very thankful to Anupriya Kumar in Schödinger's Drug Discovery Computational group for allowing us to use the Schrödinger's Small-Molecule Drug Discovery Suite and Desmond program.

ADDITIONAL INFORMATION AND DECLARATIONS

Funding

The authors received no funding for this work.

Competing Interests

Cigdem Cetin-Aluc is employed by Abdi Ibrahim Pharmaceuticals.

Author Contributions

- Yasemin Budama-Kilinc conceived and designed the experiments, analyzed the data, prepared figures and/or tables, authored or reviewed drafts of the article, and approved the final draft.

- Bahar Gok conceived and designed the experiments, performed the experiments, analyzed the data, prepared figures and/or tables, authored or reviewed drafts of the article, and approved the final draft.
- Cigdem Cetin Aluc conceived and designed the experiments, performed the experiments, analyzed the data, prepared figures and/or tables, and approved the final draft.
- Serda Kecel-Gunduz conceived and designed the experiments, analyzed the data, prepared figures and/or tables, authored or reviewed drafts of the article, and approved the final draft.

Data Availability

The following information was supplied regarding data availability:

The raw data is available in the Supplemental Files.

Supplemental Information

Supplemental information for this article can be found online at http://dx.doi.org/10.7717/peerj.15523#supplemental-information.

REFERENCES

Abdelkader A, Fathi HA, Hamad MA, Elsabahy M. 2020. Nanomedicine: a new paradigm to overcome drug incompatibilities. *Journal of Pharmacy and Pharmacology* **72(10)**:1289–1305 DOI 10.1111/jphp.13292.

Abdollahi S, Lotfipour F. 2012. PLGA-and PLA-based polymeric nanoparticles for antimicrobial drug delivery. *BioMedicine International* **3**:1–11.

Abdul Majid FA, Fadhlina A, Ismail HF, Zainol SN, Mamillapalli AK, Venkatesan V, Eswarappa R, Pillai R. 2022. Mutagenicity and safety pharmacology of a standardized antidiabetic polyherbal formulation. *Scientific Reports* **12**:7127 DOI 10.1038/s41598-022-11243-3.

Adedokun O, Ntungwe EN, Viegas C, Adesina Ayinde B, Barboni L, Maggi F, Saraiva L, Rijo P, Fonte P. 2022. Enhanced anticancer activity of hymenocardia acida stem bark extract loaded into PLGA nanoparticles. *Pharmaceuticals* **15(5)**:535 DOI 10.3390/ph15050535.

Agarwal H, Kumar SV, Rajeshkumar S. 2017. A review on green synthesis of zinc oxide nanoparticles—an eco-friendly approach. *Resource-Efficient Technologies* **3(4)**:406–413 DOI 10.1016/j.reffit.2017.03.002.

Akin D, Durak Y, Uysal A, Gunes E, Aladag MO. 2016. Assessment of antimutagenic action of Celtis glabrata Steven ex Planch. (Cannabaceae) extracts against base pair exchange and frame shift mutations on Salmonella typhimurium TA98 and TA100 strains by Ames test. *Drug and Chemical Toxicology* **39(3)**:312–321 DOI 10.3109/01480545.2015.1121273.

Al-Mahallawi AM, Abdelbary AA, Aburahma MH. 2015. Investigating the potential of employing bilosomes as a novel vesicular carrier for transdermal delivery of tenoxicam. *International Journal of Pharmaceutics* **485(1–2)**:329–340 DOI 10.1016/j.ijpharm.2015.03.033.

Al-Snafi AE. 2020. Constituents and pharmacology of *Onopordum acanthium*. *IOSR Journal of Pharmacy* **202**:3.

Arfaoui MO, Renaud J, Ghazghazi H, Boukhchina S, Mayer P. 2014. Variation in oil content, fatty acid and phytosterols profile of *Onopordum acanthium* L. during seed development. *Natural Product Research* **28(24)**:2293–2300 DOI 10.1080/14786419.2014.940944.

Azam MA, Saha N, Jupudi S. 2019. An explorative study on Staphylococcus aureus MurE inhibitor: induced fit docking, binding free energy calculation, and molecular dynamics. *Journal of Receptors and Signal Transduction* **39(1)**:45–54 DOI 10.1080/10799893.2019.1605528.

Bacanli M, Özgür E, Erdoğan H, Sarper M, Erdem O, Özkan Y. 2021. Evaluation of cytotoxic and genotoxic effects of paclitaxel-loaded PLGA nanoparticles in neuroblastoma cells. *Food and Chemical Toxicology* **154**:112323 DOI 10.1016/j.fct.2021.112323.

Baker JR, Woolfson DN, Muskett FW, Stoneman RG, Urbaniak MD, Caddick S. 2007. Protein-small molecule interactions in neocarzinostatin, the prototypical enediyne chromoprotein antibiotic. *ChemBioChem* **8**:704–717 DOI 10.1002/(ISSN)1439-7633.

Ballesteros-Ramírez R, Durán M, Fiorentino S. 2021. Genotoxicity and mutagenicity assessment of a standardized extract (P2Et) obtained from Caesalpinia spinosa. *Toxicology Reports* **8**:258–263 DOI 10.1016/j.toxrep.2020.12.024.

Barman TK, Kumar M, Mathur T, Chaira T, Ramkumar G, Kalia V, Rao M, Pandya M, Yadav AS, Das B. 2016. In vitro and in vivo activities of a bi-aryl oxazolidinone, RBx 11760, against Gram-positive bacteria. *Antimicrobial Agents and Chemotherapy* **60(12)**:7134–7145 DOI 10.1128/AAC.00453-16.

Bentrad N, Gaceb-Terrak R, Rahmania F. 2017. Identification and evaluation of antibacterial agents present in lipophilic fractions isolated from sub-products of Phoenix dactilyfera. *Natural Product Research* **31(21)**:2544–2548 DOI 10.1080/14786419.2017.1314282.

Borm PJ, Robbins D, Haubold S, Kuhlbusch T, Fissan H, Donaldson K, Schins R, Stone V, Kreyling W, Lademann J. 2006. The potential risks of nanomaterials: a review carried out for ECETOC. *Particle and Fibre Toxicology* **3(1)**:1–35 DOI 10.1186/1743-8977-3-11.

Bowers KJ, Chow DE, Xu H, Dror RO, Eastwood MP, Gregersen BA, Klepeis JL, Kolossvary I, Moraes MA, Sacerdoti FD. 2006. Scalable algorithms for molecular dynamics simulations on commodity clusters. In: *SC'06: Proceedings of the 2006 ACM/IEEE Conference on Supercomputing*, Piscataway: IEEE, 43.

Budama-Kilinc Y. 2019a. Fabrication of phloridzin loaded poly (ε-caprolactone) nanoparticles as a wound dressing material candidate for diabetic foot infections. *Science of Advanced Materials* **11(5)**:738–748 DOI 10.1166/sam.2019.3541.

Budama-Kilinc Y. 2019b. Piperine nanoparticles for topical application: preparation, characterization, in vitro and in silico evaluation. *ChemistrySelect* **4(40)**:11693–11700 DOI 10.1002/slct.201903266.

Carter TC, Ye Z, Ivacic LC, Budi N, Rose WE, Shukla SK. 2020. Association of variants in selected genes mediating host immune response with duration of Staphylococcus aureus bacteremia. *Genes & Immunity* **21(4)**:1–9 DOI 10.1038/s41435-020-0101-0.

Chaudhary H, Kumar V. 2014. Taguchi design for optimization and development of antibacterial drug-loaded PLGA nanoparticles. *International Journal of Biological Macromolecules* **64(2)**:99–105 DOI 10.1016/j.ijbiomac.2013.11.032.

Chourasiya V, Bohrey S, Pandey A. 2016. Formulation, optimization, characterization and in-vitro drug release kinetics of atenolol loaded PLGA nanoparticles using 33 factorial design for oral delivery. *Materials Discovery* **5**:1–13 DOI 10.1016/j.md.2016.12.002.

Coppi A, Davies R, Wegesser T, Ishida K, Karmel J, Han J, Aiello F, Xie Y, Corbett MT, Parsons AT. 2022. Characterization of false positive, contaminant-driven mutagenicity in impurities associated with the sotorasib drug substance. *Regulatory Toxicology and Pharmacology* **131**:105162 DOI 10.1016/j.yrtph.2022.105162.

Crossley KB, Jefferson KK, Archer GL, Fowler VG Jr. 2009. *Staphylococci in human disease*. Hoboken: John Wiley & Sons.

Desbois AP, Smith VJ. 2010. Antibacterial free fatty acids: activities, mechanisms of action and biotechnological potential. *Applied Microbiology and Biotechnology* **85(6)**:1629–1642 DOI 10.1007/s00253-009-2355-3.

Dewangan HK, Singh N, Kumar Megh S, Singh S, Lakshmi. 2022. Optimisation and evaluation of Gymnema sylvestre extract loaded polymeric nanoparticles for enhancement of in vivo efficacy and reduction of toxicity. *Journal of Microencapsulation* **39(2)**:1–11 DOI 10.1080/02652048.2022.2051625.

Dhas NL, Ige PP, Kudarha RR. 2015. Design, optimization and in-vitro study of folic acid conjugated-chitosan functionalized PLGA nanoparticle for delivery of bicalutamide in prostate cancer. *Powder Technology* **283(1)**:234–245 DOI 10.1016/j.powtec.2015.04.053.

Dorjsuren B, Chaurasiya B, Ye Z, Liu Y, Li W, Wang C, Shi D, Evans CE, Webster TJ, Shen Y. 2020. Cetuximab-coated thermo-sensitive liposomes loaded with magnetic nanoparticles and doxorubicin for targeted EGFR-expressing breast cancer combined therapy. *International Journal of Nanomedicine* **15**:8201 DOI 10.2147/IJN.S261671.

Dowling AP. 2004. Development of nanotechnologies. *Materials Today* **7(12)**:30–35 DOI 10.1016/S1369-7021(04)00628-5.

Egil AC, Ozdemir B, Gok B, Kecel-Gunduz S, Budama-Kilinc Y. 2020. Synthesis, characterization, biological activities and molecular docking of Epilobium parviflorum aqueous extract loaded chitosan nanoparticles. *International Journal of Biological Macromolecules* **161(1)**:947–957 DOI 10.1016/j.ijbiomac.2020.06.066.

Eleraky NE, Allam A, Hassan SB, Omar MM. 2020. Nanomedicine fight against antibacterial resistance: an overview of the recent pharmaceutical innovations. *Pharmaceutics* **12(2)**:142 DOI 10.3390/pharmaceutics12020142.

Ercin E, Kecel-Gunduz S, Gok B, Aydin T, Budama-Kilinc Y, Kartal M. 2022. Laurus nobilis L. essential oil-loaded PLGA as a nanoformulation candidate for cancer treatment. *Molecules* **27(6)**:1899 DOI 10.3390/molecules27061899.

Folle C, Marqués AM, Díaz-Garrido N, Espina M, Sánchez-López E, Badia J, Baldoma L, Calpena AC, García ML. 2021. Thymol-loaded PLGA nanoparticles: an efficient approach for acne treatment. *Journal of Nanobiotechnology* **19(1)**:1–21 DOI 10.1186/s12951-021-01092-z.

Friesner RA, Banks JL, Murphy RB, Halgren TA, Klicic JJ, Mainz DT, Repasky MP, Knoll EH, Shelley M, Perry JK. 2004. Glide: a new approach for rapid, accurate docking and scoring. 1. Method and assessment of docking accuracy. *Journal of Medicinal Chemistry* **47**:1739–1749 DOI 10.1021/jm0306430.

Garsiya ER, Konovalov DA, Shamilov AA, Glushko MP, Orynbasarova KK. 2019. Traditional medicine plant, *Onopordum acanthium* L. (Asteraceae): chemical composition and pharmacological research. *Plants* **8(2)**:40 DOI 10.3390/plants8020040.

Gaspar LMDAC, Dórea ACS, Droppa-Almeida D, de Mélo Silva IS, Montoro FE, Alves LL, Macedo MLH, Padilha FF. 2018. Development and characterization of PLGA nanoparticles containing antibiotics. *Journal of Nanoparticle Research* **20(11)**:289 DOI 10.1007/s11051-018-4387-z.

Gebreel RM, Edris NA, Elmofty HM, Tadros MI, El-Nabarawi MA, Hassan DH. 2021. Development and characterization of PLGA nanoparticle-laden hydrogels for sustained ocular delivery of norfloxacin in the treatment of pseudomonas keratitis: an experimental study. *Drug Design, Development and Therapy* **15**:399–418 DOI 10.2147/DDDT.S293127.

Gheffar C, Le H, Jouenne T, Schaumann A, Corbière A, Vaudry D, LeCerf D, Karakasyan C. 2021. Antibacterial activity of ciprofloxacin-loaded poly (lactic-co-glycolic acid)-nanoparticles

against Staphylococcus aureus. *Particle & Particle Systems Characterization* **38(1)**:2000253 DOI 10.1002/ppsc.202000253.

Halgren TA, Murphy RB, Friesner RA, Beard HS, Frye LL, Pollard WT, Banks JL. 2004. Glide: a new approach for rapid, accurate docking and scoring. 2. Enrichment factors in database screening. *Journal of Medicinal Chemistry* **47**:1750–1759 DOI 10.1021/jm030644s.

Hamzaoui A, Laraba-Djebari F. 2021. Development and evaluation of polymeric nanoparticles as a delivery system for snake envenoming prevention. *Biologicals* **70(5)**:44–52 DOI 10.1016/j.biologicals.2021.01.003.

Harder E, Damm W, Maple J, Wu C, Reboul M, Xiang JY, Wang L, Lupyan D, Dahlgren MK, Knight JL. 2016. OPLS3: a force field providing broad coverage of drug-like small molecules and proteins. *Journal of Chemical Theory and Computation* **12(1)**:281–296 DOI 10.1021/acs.jctc.5b00864.

Hariharan S, Bhardwaj V, Bala I, Sitterberg J, Bakowsky U, Kumar MR. 2006. Design of estradiol loaded PLGA nanoparticulate formulations: a potential oral delivery system for hormone therapy. *Pharmaceutical Research* **23(1)**:184–195 DOI 10.1007/s11095-005-8418-y.

Hastings J, Owen G, Dekker A, Ennis M, Kale N, Muthukrishnan V, Turner S, Swainston N, Mendes P, Steinbeck C. 2016. ChEBI in 2016: improved services and an expanding collection of metabolites. *Nucleic Acids Research* **44(D1)**:D1214–D1219 DOI 10.1093/nar/gkv1031.

Hill LE, Taylor TM, Gomes C. 2013. Antimicrobial efficacy of poly (DL-lactide-co-glycolide) (PLGA) nanoparticles with entrapped cinnamon bark extract against listeria monocytogenes and salmonella typhimurium. *Journal of Food Science* **78(4)**:N626–N632 DOI 10.1111/1750-3841.12069.

ISO. 2009. *10993–5: 2009 Biological evaluation of medical devices—part 5: tests for in vitro cytotoxicity*. Geneva: International Organization for Standardization. *Available at https://www.iso.org/standard/36406.html*.

Jummes B, Sganzerla WG, da Rosa CG, Noronha CM, Nunes MR, Bertoldi FC, Barreto PLM. 2020. Antioxidant and antimicrobial poly-ε-caprolactone nanoparticles loaded with Cymbopogon martinii essential oil. *Biocatalysis and Agricultural Biotechnology* **23**:101499 DOI 10.1016/j.bcab.2020.101499.

Karimi SM, Sankian M, Khademi F, Tafaghodi M. 2016. Chitosan (CHT) and trimethylchitosan (TMC) nanoparticles as adjuvant/delivery system for parenteral and nasal immunization against Mycobacterium tuberculosis (MTb) ESAT-6 antigen. *Nanomedicine Journal* **3**:223–229 DOI 10.22038/NMJ.2016.7577.

Karl C, Mueller G, Pedersen PA. 1976. On the phytochemistry of the flowers of Onopordon acanthium L. (Cotton thistle). *Deutsche Apotheker-Zeitung* **11**:57–59.

Khalilov L, Khalilova A, Shakurova E, Nuriev I, Kachala V, Shashkov A, Dzhemilev U. 2003. PMR and 13 C NMR spectra of biologically active compounds. XII. Taraxasterol and its acetate from the aerial part of *Onopordum acanthium*. *Chemistry of Natural Compounds* **39(3)**:285–288 DOI 10.1023/A:1025478720459.

Khan N, Khan I, Azam S, Ahmad F, Khan HA, Shah A, Ullah M. 2021. Potential cytotoxic and mutagenic effect of Pinus wallichiana, Daphne oleiodes and Bidens chinensis. *Saudi Journal of Biological Sciences* **28(8)**:4793–4799 DOI 10.1016/j.sjbs.2021.05.005.

Khoshkhounejad M, Sharifian M, Assadian H, Afshar MS. 2021. Antibacterial effectiveness of diluted preparations of intracanal medicaments used in regenerative endodontic treatment on dentin infected by bacterial biofilm: An ex vivo investigation. *Dental Research Journal* **18**:37.

Kim JK, Kim HJ, Chung J-Y, Lee J-H, Young S-B, Kim Y-H. 2014. Natural and synthetic biomaterials for controlled drug delivery. *Archives of Pharmacal Research* **37(1)**:60–68 DOI 10.1007/s12272-013-0280-6.

Koc S, Isgor BS, Isgor YG, Shomali Moghaddam N, Yildirim O. 2015. The potential medicinal value of plants from Asteraceae family with antioxidant defense enzymes as biological targets. *Pharmaceutical Biology* **53(5)**:746–751 DOI 10.3109/13880209.2014.942788.

Kost B, Svyntkivska M, Brzeziński M, Makowski T, Piorkowska E, Rajkowska K, Kunicka-Styczyńska A, Biela T. 2020. PLA/β-CD-based fibres loaded with quercetin as potential antibacterial dressing materials. *Colloids and Surfaces B: Biointerfaces* **190(5)**:110949 DOI 10.1016/j.colsurfb.2020.110949.

Kumari V, Tyagi P, Sangal A. 2022. In-Vitro kinetic release study of illicium verum (Chakraphool) polymeric nanoparticles. *Materials Today: Proceedings* **60**:14–20 DOI 10.1016/j.matpr.2021.11.014.

Kumari A, Yadav SK, Yadav SC. 2010. Biodegradable polymeric nanoparticles based drug delivery systems. *Colloids and Surfaces B: Biointerfaces* **75(1)**:1–18 DOI 10.1016/j.colsurfb.2009.09.001.

Kusumah D, Wakui M, Murakami M, Xie X, Yukihito K, Maeda I. 2020. Linoleic acid, α-linolenic acid, and monolinolenins as antibacterial substances in the heat-processed soybean fermented with Rhizopus oligosporus. *Bioscience, Biotechnology, and Biochemistry* **84(6)**:1285–1290 DOI 10.1080/09168451.2020.1731299.

Labreure R, Sona A, Turos E. 2019. Anti-methicillin resistant Staphylococcus aureus (MRSA) nanoantibiotics. *Frontiers in Pharmacology* **10**:1121 DOI 10.3389/fphar.2019.01121.

Malewicz NM, Rattray Z, Oeck S, Jung S, Escamilla-Rivera V, Chen Z, Tang X, Zhou J, LaMotte RH. 2022. Topical capsaicin in poly (lactic-co-glycolic) acid (PLGA) nanoparticles decreases acute itch and heat pain. *International Journal of Molecular Sciences* **23(9)**:5275 DOI 10.3390/ijms23095275.

Maron DM, Ames BN. 1983. Revised methods for the Salmonella mutagenicity test. *Mutation Research/Environmental Mutagenesis and Related Subjects* **113(3–4)**:173–215 DOI 10.1016/0165-1161(83)90010-9.

Matthaus B, Ozcan M, Al-Juhaimi F. 2014. Fatty acid, tocopherol, and mineral contents of *Onopordum acanthium* seed and oil. *Chemistry of Natural Compounds* **50(4)**:1092–1093 DOI 10.1007/s10600-014-1166-7.

McCaig LF, McDonald LC, Mandal S, Jernigan DB. 2006. Staphylococcus aureus-associated skin and soft tissue infections in ambulatory care. *Emerging Infectious Diseases* **12(11)**:1715–1723 DOI 10.3201/eid1211.060190.

Mohammadi G, Valizadeh H, Barzegar-Jalali M, Lotfipour F, Adibkia K, Milani M, Azhdarzadeh M, Kiafar F, Nokhodchi A. 2010. Development of azithromycin-PLGA nanoparticles: physicochemical characterization and antibacterial effect against Salmonella typhi. *Colloids and Surfaces B: Biointerfaces* **80(1)**:34–39 DOI 10.1016/j.colsurfb.2010.05.027.

Móricz AM, Krüzselyi D, Alberti Á, Darcsi A, Horváth G, Csontos P, Béni S, Ott PG. 2017. Layer chromatography-bioassays directed screening and identification of antibacterial compounds from Scotch thistle. *Journal of Chromatography A* **1524**:266–272 DOI 10.1016/j.chroma.2017.09.062.

Mortelmans K, Zeiger E. 2000. The Ames Salmonella/microsome mutagenicity assay. *Mutation Research/Fundamental and Molecular Mechanisms of Mutagenesis* **455(1–2)**:29–60 DOI 10.1016/S0027-5107(00)00064-6.

Mukerjee A, Vishwanatha JK. 2009. Formulation, characterization and evaluation of curcumin-loaded PLGA nanospheres for cancer therapy. *Anticancer Research* **29**:3867–3875.

Nabavizadeh MR, Moazzami F, Gholami A, Mehrabi V, Ghahramani Y. 2022. Cytotoxic effect of nano fast cement and ProRoot mineral trioxide aggregate on L-929 fibroblast cells: an in vitro study. *Journal of Dentistry* **23**:13 DOI 10.30476/DENTJODS.2021.87208.1239.

Nemati S, Mohammad Rahimi H, Hesari Z, Sharifdini M, Jalilzadeh Aghdam N, Mirjalali H, Zali MR. 2022. Formulation of neem oil-loaded solid lipid nanoparticles and evaluation of its anti-Toxoplasma activity. *BMC Complementary Medicine and Therapies* **22**:122 DOI 10.1186/s12906-022-03607-z.

Ni J, Liu Y, Hussain T, Li M, Liang Z, Liu T, Zhou X. 2021. Recombinant ArgF PLGA nanoparticles enhances BCG induced immune responses against Mycobacterium bovis infection. *Biomedicine & Pharmacotherapy* **137**:111341 DOI 10.1016/j.biopha.2021.111341.

Nija B, Rasheed A, Kottaimuthu A. 2020. Development, characterization, and pharmacological investigation of sesamol and thymol conjugates of mefenamic acid. *Journal of Evolution of Medical and Dental Sciences* **9(52)**:3909–3917 DOI 10.14260/jemds/2020/857.

Olsson MH, Søndergaard CR, Rostkowski M, Jensen JH. 2011. PROPKA3: consistent treatment of internal and surface residues in empirical p K a predictions. *Journal of Chemical Theory and Computation* **7(2)**:525–537 DOI 10.1021/ct100578z.

Omokhua AG, Abdalla MA, Van Staden J, McGaw LJ. 2018. A comprehensive study of the potential phytomedicinal use and toxicity of invasive Tithonia species in South Africa. *BMC Complementary and Alternative Medicine* **18**:272 DOI 10.1186/s12906-018-2336-0.

Paszel-Jaworska A, Romaniuk A, Rybczynska M. 2014. Molecular mechanisms of biological activity of oleanolic acid-A source of inspiration for a new drugs design. *Mini-Reviews in Organic Chemistry* **11(3)**:330–342 DOI 10.2174/1570193X1103140915111839.

Pieper S, Langer K. 2017. Doxorubicin-loaded PLGA nanoparticles-a systematic evaluation of preparation techniques and parameters*. *Materials Today: Proceedings* **4**:S188–S192 DOI 10.1016/j.matpr.2017.09.185.

Radwan R, Abdelkader A, Fathi HA, Elsabahy M, Fetih G, El-Badry M. 2021. Development and evaluation of letrozole-loaded hyaluronic acid/chitosan-coated poly (d, l-lactide-co-glycolide) nanoparticles. *Journal of Pharmaceutical Innovation* **17**:1–12 DOI 10.1007/s12247-021-09538-5.

Razura-Carmona FF, Perez-Larios A, Sáyago-Ayerdi SG, Herrera-Martínez M, Sánchez-Burgos JA. 2022. Biofunctionalized nanomaterials: alternative for encapsulation process enhancement. *Polysaccharides* **3(2)**:411–425 DOI 10.3390/polysaccharides3020025.

Roberts R, Smyth JW, Will J, Roberts P, Grek CL, Ghatnekar GS, Sheng Z, Gourdie RG, Lamouille S, Foster EJ. 2020. Development of PLGA nanoparticles for sustained release of a connexin43 mimetic peptide to target glioblastoma cells. *Materials Science and Engineering C* **108**:110191 DOI 10.1016/j.msec.2019.110191.

Ruane KM, Lloyd AJ, Fülöp V, Dowson CG, Barreteau H, Boniface A, Dementin S, Blanot D, Mengin-Lecreulx D, Gobec S. 2013. Specificity determinants for lysine incorporation in Staphylococcus aureus peptidoglycan as revealed by the structure of a MurE enzyme ternary complex. *Journal of Biological Chemistry* **288(46)**:33439–33448 DOI 10.1074/jbc.M113.508135.

Samling BA, Assim Z, Tong W-Y, Leong C-R, Ab Rashid S, Kamal NNSNM, Muhamad M, Tan W-N. 2022. Cynometra cauliflora essential oils loaded-chitosan nanoparticles: evaluations of their antioxidant, antimicrobial and cytotoxic activities. *International Journal of Biological Macromolecules* **210**:742–751 DOI 10.1016/j.ijbiomac.2022.04.230.

Sastry GM, Adzhigirey M, Day T, Annabhimoju R, Sherman W. 2013. Protein and ligand preparation: parameters, protocols, and influence on virtual screening enrichments. *Journal of Computer-Aided Molecular Design* **27(3)**:221–234 DOI 10.1007/s10822-013-9644-8.

Schrödinger L. 2021. *Schrödinger release 2021-4: desmond molecular dynamics system*. New York, NY, USA: DE Shaw Research.

Shabestarian H, Tabrizi MH, Es-Haghi A, Khadem F. 2021. The Brassica napus extract (BNE)-loaded PLGA nanoparticles as an early necroptosis and late apoptosis inducer in human MCF-7 breast cancer cells. *Nutrition and Cancer* **74(7)**:1–10 DOI 10.1080/01635581.2021.2008986.

Sharma A, Sanjeev K, Selvanathan VM, Sekar M, Harikrishnan N. 2022. The evaluation of cytotoxicity and cytokine IL-6 production of root canal sealers with and without the incorporation of simvastatin: an invitro study. *BMC Oral Health* **22**:6 DOI 10.1186/s12903-022-02039-y.

Shen S, Wu Y, Liu Y, Wu D. 2017. High drug-loading nanomedicines: progress, current status, and prospects. *International Journal of Nanomedicine* **12**:4085 DOI 10.2147/IJN.

Shu Y, Liu Y, Li L, Feng J, Lou B, Zhou X, Wu H. 2011. Antibacterial activity of quercetin on oral infectious pathogens. *African Journal of Microbiology Research* **5**:5358–5361 DOI 10.5897/AJMR11.849.

Sibbald M, Ziebandt A, Engelmann S, Hecker M, De Jong A, Harmsen H, Raangs G, Stokroos I, Arends J, Dubois J. 2006. Mapping the pathways to staphylococcal pathogenesis by comparative secretomics. *Microbiology and Molecular Biology Reviews* **70(3)**:755–788 DOI 10.1128/MMBR.00008-06.

Silva ISDM, Santos RFEPD, Melo TDVC, Silva AJCD, Sarmento PDA, Lúcio IML, Campesatto EA, Padilha FF, Conserva LM, Bastos MLDA. 2014. In vitro biological potential of Guanxuma-of-Horn [Sebastiania corniculata (Vahl) Mull. Arg.] in infection control. *Journal of Chemical and Pharmaceutical Research,* Rajasthan **6(4)**:663–669.

Simon A, Moreira MLA, Costa IFDJB, de Sousa VP, Rodrigues CR, Sisnande T, do Carmo FA, Leal ICR, Dos Santos KRN, da Silva LCRP. 2020. Vancomycin-loaded nanoparticles against vancomycin intermediate and methicillin resistant Staphylococcus aureus strains. *Nanotechnology* **31(37)**:375101 DOI 10.1088/1361-6528/ab97d7.

Sousa F, Cruz A, Fonte P, Pinto IM, Neves-Petersen MT, Sarmento B. 2017. A new paradigm for antiangiogenic therapy through controlled release of bevacizumab from PLGA nanoparticles. *Scientific Reports* **7**:3736 DOI 10.1038/s41598-017-03959-4.

Taherkhani M. 2015. Chemical constituents and in vitro anticancer, cytotoxic, mutagenic and antimutagenic activities of Artemisia diffusa. *Pharmaceutical Chemistry Journal* **48(11)**:727–732 DOI 10.1007/s11094-015-1182-3.

Tassa C, Duffner JL, Lewis TA, Weissleder R, Schreiber SL, Koehler AN, Shaw SY. 2010. Binding affinity and kinetic analysis of targeted small molecule-modified nanoparticles. *Bioconjugate Chemistry* **21(1)**:14–19 DOI 10.1021/bc900438a.

Tsai W-C, Chang H-C, Tseng Y-H, Yin H-Y, Liao J-W, Agrawal DC, Wen H-W. 2020. Toxicity evaluation of water extract of tissue-cultured Taraxacum formosanum by acute, subacute administration, and Ames test. *Electronic Journal of Biotechnology* **45(8)**:38–45 DOI 10.1016/j.ejbt.2020.04.001.

Tyumkina T, Nuriev I, Khalilov L, Akhmetova V, Dzhemilev U. 2009. PMR and 13 C NMR spectra of biologically active compounds. XIII.* Structure and stereochemistry of a new phenylpropanoid glycoside isolated from *Onopordum acanthium* seeds. *Chemistry of Natural Compounds* **45(1)**:61–65 DOI 10.1007/s10600-009-9254-9.

Wang Y, Ren B, Zhou X, Liu S, Zhou Y, Li B, Jiang Y, Li M, Feng M, Cheng L. 2017. Growth and adherence of Staphylococcus aureus were enhanced through the PGE2 produced by the activated COX-2/PGE2 pathway of infected oral epithelial cells. *PLOS ONE* **12**:e0177166 DOI 10.1371/journal.pone.0177166.

Wang S, Yao J, Zhou B, Yang J, Chaudry MT, Wang M, Xiao F, Li Y, Yin W. 2018. Bacteriostatic effect of quercetin as an antibiotic alternative in vivo and its antibacterial mechanism in vitro. *Journal of Food Protection* **81(1)**:68–78 DOI 10.4315/0362-028X.JFP-17-214.

Yang S-C, Tseng C-H, Wang P-W, Lu P-L, Weng Y-H, Yen F-L, Fang J-Y. 2017. Pterostilbene, a methoxylated resveratrol derivative, efficiently eradicates planktonic, biofilm, and intracellular MRSA by topical application. *Frontiers in Microbiology* **8**:1103 DOI 10.3389/fmicb.2017.01103.

Ying Z, Ruotao T, Haili W, Shuqin L, Linxiu B, Xuemin L, Qing L. 2022. A study of the genetic and prenatal developmental toxicity potential of lithothamnion sp. *Drug and Chemical Toxicology* **45**:1644–1651 DOI 10.1080/01480545.2020.1853150.

Zare K, Nazemyeh H, Lotfipour F, Farabi S, Ghiamirad M, Barzegari A. 2014. Antibacterial activity and total phenolic content of the Onopordon acanthium L. seeds. *Pharmaceutical Sciences* **20**:6–11.

Zeiger E. 2019. The test that changed the world: the Ames test and the regulation of chemicals. *Mutation Research/Genetic Toxicology and Environmental Mutagenesis* **841**:43–48 DOI 10.1016/j.mrgentox.2019.05.007.

Zhang X, Levia DF, Ebikade EO, Chang J, Vlachos DG, Wu C. 2022. The impact of differential lignin S/G ratios on mutagenicity and chicken embryonic toxicity. *Journal of Applied Toxicology* **42(3)**:423–435 DOI 10.1002/jat.4229.

Zhang L, Pornpattananangkul D, Hu C-M, Huang C-M. 2010. Development of nanoparticles for antimicrobial drug delivery. *Current Medicinal Chemistry* **17(6)**:585–594 DOI 10.2174/092986710790416290.

Zhang J, Sun H, Gao C, Wang Y, Cheng X, Yang Y, Gou Q, Lei L, Chen Y, Wang X. 2021. Development of a chitosan-modified PLGA nanoparticle vaccine for protection against Escherichia coli K1 caused meningitis in mice. *Journal of Nanobiotechnology* **19(1)**:1–15 DOI 10.1186/s12951-021-00812-9.

Zhao Y-L, Su M, Shang J-H, Wang X, Bao G-L, Ma J, Sun Q-D, Yuan F, Wang J-K, Luo X-D. 2020. Genotoxicity and safety pharmacology studies of indole alkaloids extract from leaves of Alstonia scholaris (L.) R. Br. *Natural Products and Bioprospecting* **10(3)**:119–129 DOI 10.1007/s13659-020-00242-4.